symmetry

MDPI

Article

Comprehensive Study of Electrode Effect in Metal/$CuInP_2S_6$/Metal Heterostructures

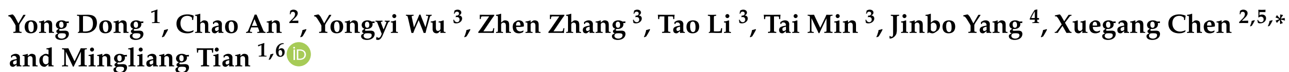

Yong Dong [1], Chao An [2], Yongyi Wu [3], Zhen Zhang [3], Tao Li [3], Tai Min [3], Jinbo Yang [4], Xuegang Chen [2,5,*] and Mingliang Tian [1,6]

[1] School of Physics and Optoelectronic Encineering, Anhui University, Hefei 230601, China
[2] Institutes of Physical Science and Information Technology, Anhui University, Hefei 230601, China
[3] Center for Spintronics and Quantum Systems, State Key Laboratory for Mechanical Behavior of Materials, Department of Materials Science and Engineering, Xi'an Jiaotong University, Xi'an 710049, China
[4] State Key Laboratory for Mesoscopic Physics, School of Physics, Peking University, Beijing 100871, China
[5] Center of Free Electron Laser & High Magnetic Field, Anhui University, Hefei 230601, China
[6] Anhui Province Key Laboratory of Condensed Matter Physics at Extreme Conditions, High Magnetic Field Laboratory, Chinese Academy of Sciences, Hefei 230031, China
* Correspondence: xgchen@ahu.edu.cn

Abstract: The layered van der Waals $CuInP_2S_6$ (CIPS) features interesting functional behaviors, including reversible ferroelectric polarization, Cu ion migration, negative capacitance effect, etc. Here, the CIPS flakes were exfoliated from the CVT-grown high-quality single crystals, which were fabricated into metal/CIPS/metal heterostructures by conventional photolithography. It was found that the CIPS flakes persisted in the dominant out-of-plane polarization and the minor in-plane polarization. Clear hysteresis current–voltage (I–V) loops, as well as the rectifying character, were revealed in metal/CIPS/metal heterostructures, indicating the potential application as a memory device. Additionally, the different metal electrode could significantly modulate the Schottky-like barrier at metal/CIPS interfaces, resulting in symmetric or asymmetric I–V loops. The complicated I–V curves may have originated from the voltage-induced Cu ion migration, reversible ferroelectric polarization, and carrier (ion) trapping/detrapping. This work may facilitate the metal electrode selection for the ferroelectric CIPS-based device application.

Keywords: van der Waals $CuInP_2S_6$; metal electrode; ferroelectric polarization; copper migration

Citation: Dong, Y.; An, C.; Wu, Y.; Zhang, Z.; Li, T.; Min, T.; Yang, J.; Chen, X.; Tian, M. Comprehensive Study of Electrode Effect in Metal/$CuInP_2S_6$/Metal Heterostructures. *Symmetry* **2023**, *15*, 966. https://doi.org/10.3390/sym15050966

Academic Editor: Vladimir A. Stephanovich

Received: 6 March 2023
Revised: 5 April 2023
Accepted: 13 April 2023
Published: 24 April 2023

Copyright: © 2023 by the authors. Licensee MDPI, Basel, Switzerland. This article is an open access article distributed under the terms and conditions of the Creative Commons Attribution (CC BY) license (https://creativecommons.org/licenses/by/4.0/).

1. Introduction

Ferroelectric materials persist in stable and reversible polarization, which can be used in various applications, such as ferroelectric field effect transistors (Fe-FETs) [1,2], ferroelectric tunnel junctions [3], ferroelectric diodes [4–6], ferroelectric-based flexible devices [7,8], photodetectors [9], etc. Among them, ferroelectric diodes based on resistance switching (RS) behavior have been extensively studied because of their simple structure as well as their potential applications. Various perovskite oxides are used in ferroelectric-related devices, such as $BiFeO_3$ [10], $Pb(Zr,Ti)O_3$ (PZT) [11], $BaTiO_3$ [12], etc. Recently, due to the development of the material exploration, two-dimensional van der Waals (vdW) materials have attracted much attention because of their unique mechanical, thermal, optical, and electrical properties. $CuInP_2S_6$, one of the extensively studied vdW materials, is well known for its unique room-temperature ferroelectricity, with the Curie temperature of 315 K [13]. The switchable piezoelectric response of a 4 nm (six layers) CIPS flake has been reported [14], verifying the room temperature ferroelectric polarization. CIPS-based ferroelectric devices have also been widely investigated, such as ferroelectric diodes with vertical and horizontal metal/ferroelectric/metal (MFM) structures that exhibit excellent resistance switching (RS) behavior [5,6]. Generally, different metal electrodes in metal/ferroelectric/metal heterostructures have diverse work functions, affinity energy, and charge screening length,

etc., resulting in symmetric/asymmetric Schottky-like barriers as well as hysteresis current–voltage (I–V) curves [15,16]. The voltage-driven ion migration (copper ion migration energy ~0.65–0.75 eV) [17,18] of ferroelectric CIPS could greatly affect the Schottky-like barrier, as well as the space charge region at the metal/CIPS interface [19]. Consequently, the performance of a ferroelectric device is decided by both the metal electrode and the ferroelectric CIPS. Previously, the vertical Au/CIPS/Ti ferroelectric diodes showed a clear rectifying character with RS behavior, which was attributed to the modulation of barrier height at the interface due to the ion migration and charge trapping/detrapping [5]. Few works have related the metal electrode effect, as well as the ion migration in CIPS. Therefore, it is important to clarify the metal electrode effect and ion migration on the Schottky-like barrier, which can facilitate the application of ferroelectric materials.

In this work, the CIPS flakes were exfoliated from the chemical vapor transport (CVT) -grown high-quality single crystals. Then, they were fabricated into metal/CIPS/metal (Ti and Au metal electrodes) heterostructures by conventional photolithography. The dominant out-of-plane polarization of CIPS was characterized by piezoresponse force microscopy (PFM). The clear hysteresis I–V loops, as well as the rectifying character, were measured in metal/CIPS/metal heterostructures, indicating the potential application as a nonvolatile memory device. Different metal electrodes could significantly modulate the Schottky-like barrier at metal/CIPS interfaces, resulting in the symmetric I–V loops in Au/CIPS/Au and the asymmetric I–V loops in Ti/CIPS/Au. The observed complicated I–V curves may have originated from the voltage-induced Cu ion migration, reversible ferroelectric polarization, and carrier (ion) trapping/detrapping. The higher Schottky-like barrier was observed in the Ti/CIPS interface, which could facilitate the appearance of hysteresis I–V loops in asymmetric metal/CIPS/metal structures. This work may facilitate the metal electrode selection for the ferroelectric CIPS-based device application.

2. Materials and Methods

The high-quality single crystal CIPS was grown by the CVT method [20,21]. The precursors of Cu, In, P, and S powders were mixed in stoichiometric proportions of 1:1:2:6 and sealed in vacuum quartz ampoules, with iodine as the transport agent (2 mg/cm^3). Then, it was placed in a two-zone horizontal tube furnace for 168 h, with the hot and cold zones set at 750 and 650 °C, respectively. After sufficient reaction, the yellow bulk CIPS was collected from the tube after the tube furnace was cooled.

The CIPS flakes were mechanically exfoliated on the SiO_2/Si substrates from the as-grown CIPS single crystals. Then, the CIPS flakes were dry-transferred to the bottom Au electrodes (Au (20 nm)/Ti (5 nm)/SiO_2 (300 nm)/Si), which were fabricated by standard photolithography patterning followed by the electron beam evaporation and lift-off process. Finally, the top electrodes of Au/Ti (60 nm/20 nm) or Au (80 nm) were fabricated on CIPS flakes by a standard optical lithography method, forming the cross matrix devices.

The Raman spectra profiles of the exfoliated CIPS flakes were recorded in a wavenumber range of 50 cm^{-1} to 100 cm^{-1} at room temperature using a commercial Renishaw spectrometer system (λ = 532 nm). The crystal structure was characterized by X-ray diffraction (XRD) using a PAnalytical X' Pert MRD diffractometer with Cu Kα radiation. The morphology and piezoresponse of CIPS were performed using a commercial atomic force microscope (Asylum Research MFP-3D) with a standard conductive probe manufactured by NanoSensors; a Pt/Ir-coated silicon-based probe with a tip radius of ~25 nm. The in situ VPFM and lateral LPFM imaging of CIPS sheets prepared on n-doped Si substrates under an AC voltage (V_{AC} = 0.1–0.5 V)-driven probe tip was performed. All PFM measurements were performed at ambient humidity and temperature. The I–V characteristics were tested in a homemade Labview-controlled system with a Keithley 2636B source measure meter. The positive voltage was defined as a voltage applied on the top Au electrode. All I–V measurements were performed at room temperature.

3. Results and Discussions

The $CuInP_2S_6$ was one of the representative two-dimensional ferroelectric materials that reserved the ferroelectric ordering until its Curie temperature of 315 K (T_C~315 K) [22]. The CVT-grown CIPS crystals in this work consisted of sulfur octahedral frameworks stacked layer by layer. The frameworks in the layers formed different triangular sublattices, which were filled by Cu, In, and P–P triangular pairs, respectively (shown in Figure 1a,b). The framework layers were weakly coupled by the vdW interaction. The off-center shifting of the Cu sublattice and the cation migration in the In sublattice were strongly related to the spontaneous polarization in CIPS [23].

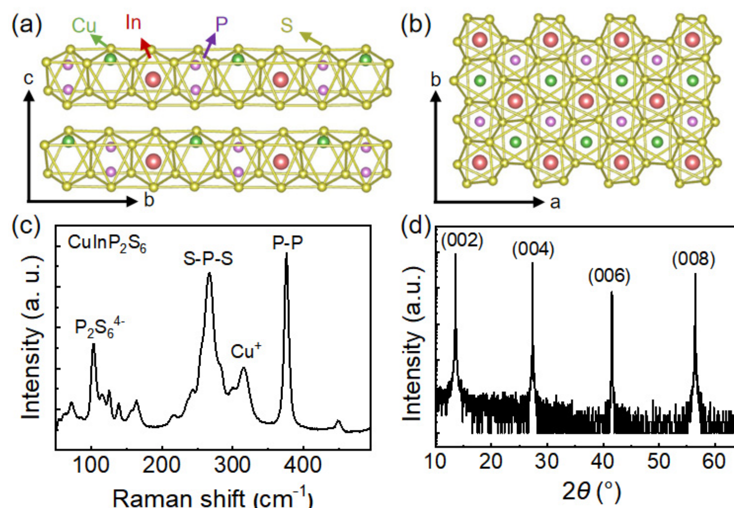

Figure 1. Crystal structure and characterization of CIPS. (**a**) The side view and (**b**) top view of the crystal structure of CIPS with a vdW gap between the layers. Raman spectra (**c**) and X-ray diffraction patterns (**d**) of CIPS at room-temperature.

The as-grown crystals were characterized by Raman spectroscopy and X-ray diffraction. The typical Raman-spectrum profile of an exfoliated flake collected with 532 nm laser excitation is shown in Figure 1c. Clear characteristic Raman peaks of CIPS could be identified, corroborating the ferroelectric phase of the CVT-grown crystals. The peaks at 315 cm^{-1} and 102 cm^{-1} corresponded to the vibrations of cation (Cu^+) and anion ($P_2S_6{}^{4-}$), respectively. The peak at 266 cm^{-1} was related to S-P-S vibrations, while the peak at 376 cm^{-1} was from the P-P stretching [1,24,25]. Multiple peaks between 125 cm^{-1} and 139 cm^{-1} were closely connected to the anion vibrational modes of the $CuInP_2S_6$-$In_{4/3}P_2S_6$ phase [26]. It was noteworthy that the Raman peaks revealed the existence of ferroelectric dipole at room temperature in CIPS flakes.

Figure 1d displays the X-ray diffraction patterns (XRD) of bulk CIPS single crystals. Only diffraction peaks of (00*l*) were observed [21,27]. The corresponding out-of-plane lattice constant could be calculated by the Bragg diffraction relation $2d_{hkl}sin\theta = \lambda$, where the λ and d_{hkl} are the wavelength of X-ray (1.5406 Å) and the interplanar spacing of (*hkl*) plane, respectively. The calculated d_{002} was 6.53 Å, namely the out-of-plane lattice c = 13.06 Å, which was similar to the previous report [28].

Since the high-quality CIPS single crystal was prepared, it was natural to show the evidence of ferroelectricity of the exfoliated-CIPS flakes. Here, we characterized the ferroelectricity of CIPS flakes in dual AC resonance tracking (DART) mode, using piezoresponse force microscopy (PFM). The CIPS flake was exfoliated on n-type heavily doped Si substrates by a conventional mechanical exfoliation method. Figure 2a displays a typical topography of exfoliated ~110 nm CIPS flakes. The out-of-plane PFM hysteresis response was measured in order to obtain a quantitative characterization of the CIPS flakes, as shown in Figure 2b. A clear-phase hysteresis loop with a 180° phase difference was obtained, revealing the out-of-plane three-dimensional ferroelectric ordering in CIPS. The coercivities

were +3.5 V (+320 kV/cm) and −5.0 V (−455 kV/cm), which was slightly larger than that of ~200 kV/cm reported in the literature [23]. Generally, the PFM amplitude reflected the strength of the local piezoelectric response of the sample, while the PFM phase represented the direction of polarization in each domain. CIPS is a typical out-of-plane ferroelectric material; however, Hong et al. found that it contains the in-plane polarization above a critical thickness (~90 nm) [27]. Therefore, both vertical-PFM (VPFM) and lateral-PFM (LPFM) measurements were carried out to testify the dominant out-of-plane polarization and minor in-plane polarization, further proving the high quality of the CIPS crystals. Figure 2c,d show the out-of-plane PFM response, while Figure 2e,f show the in-plane PFM response of the CIPS sample. Obviously, the VPFM signals showed a strong contrast between the two polarization states, implying the robust spontaneous out-of-plane polarization. On the contrary, the LPFM signals displayed the blurred pieces, corresponding with the weak in-plane polarization. In addition, there was inevitably a Cu-deficient $In_{4/3}P_2S_6$ (IPS) phase due to the coherent spinodal decomposition of Cu during the crystal preparation, which was a centrosymmetric structure with no piezoelectricity or ferroelectricity [29]. Therefore, some regions of weak response could be seen in the amplitude figure.

The sandwiched matrix devices of metal/CIPS/metal were fabricated to study the I–V characteristics. Here, we chose mechanically exfoliated thin CIPS flakes with a thickness of ~30–60 nm as the interlayer material due to its robust switchable polarization [14,23]. Figure 3a shows a schematic diagram with a titanium top electrode and a gold bottom electrode for the typical two terminals I–V test; the corresponding optical image of the matrix device is shown as inset. The typical characteristic I–V curves shown in Figure 3b were measured at various voltages (ramping rate of 0.5 V/s). The sweeping directions are indicated by arrows in Figure 3b. Generally, the measured current was in the picoampere level, corroborating the comparative insulating nature of CIPS. The I–V curve showed a tiny current variation (~0.5 pA) under a voltage of ±4 V, while a large current change (5 pA) with a clear hysteresis loop was observed under the voltage of ±5 V. The I–V curve also displayed a rectifying character, which was an indication of a Schottky-like barrier formed at the metal/CIPS interface. The hysteresis loop feature of the I–V curve displayed a typical resistive switching behavior, which was classified as volatile case for our metal/CIPS/metal stack. The current switching ratio (I_{on}/I_{off}), defined as the current difference at +3.4 V between the voltage ramping up and down at the positive voltage branch, gradually increased from 1.21 under ±4 V to 32.06 under ±5 V [5,14]. The I–V curves with hysteresis loop and rectifying character appeared with a slow voltage ramping rate (<1.0 V/s), as shown in Figure 3c, which was absent at a fast voltage ramping rate (≥2.0 V/s).

Generally, the carriers dominated the conducting properties in the common materials. As for some layered ferroelectric materials, the polar atomic migrations could be flipped back and forth within the double-well potential by reversing a small electric field (voltage), namely the reversible switching of the ferroelectric polarization, while a large electric field (voltage) could overcome the energy barrier for ion migrations between unit cells, resulting in the ions moving without being bound [30]. Therefore, the van der Waals ferroelectric material properties were strongly dependent on the applied voltage amplitude and duration [31,32]. As for the conduction in CIPS, it was not only the usual carriers that dominated the transport properties, but the voltage-driven copper ion migration also had some contributions. Consequently, the small voltage displayed a tiny current, corresponding to the intrinsic low carrier density in CIPS. As the voltage amplitude increased, it seemed the energy barrier of ion migration (~0.65–0.75 eV) was reached, resulting in the significant rising of current as well as the appearance of an I–V hysteresis loop. The hysteresis loop could originate from the trapping/detrapping of carriers/ions [33]. The switching ratio increased with an increasing sweep speed, which may have resulted from the higher electric field further driving the alignment of electric dipoles in the copper and indium sublattice [14]. Figure 3d shows the schematic energy diagram in Ti/CIPS/Au ferroelectric diodes under different electric fields. The incomplete screening of the two

different electrodes caused an energy band bending at the metal/interface, which could modulate the Schottky-like barrier height (SBH) [16]. The asymmetric I–V curve may have originated from the different work function and affinity energy between titanium and gold, as well as the different band bending effect at the Ti/CIPS and Au/CIPS interface and the voltage-induced polarization effect [5]. Since the characteristic I–V curve revealed a Schottky-like behavior, the Schottky-like barrier energy could be extracted by the relation $I(V) = AT^2 \exp\left(-\frac{q\varphi_b}{k_B T}\right)\left(\exp\left(\frac{qV}{k_B T}\right) - 1\right)$, where A, T, q, and k_B are the perfector constant, temperature, electro charge, and Boltzmann constant, respectively. The calculated Schottky-like barrier heights were 0.926 eV and 1.096 eV at the Au/CIPS and Ti/CIPS interfaces, which were slightly larger than the copper migration energy. Clearly, the Schottky-like barrier of Ti/CIPS was slightly larger than that of Au/CIPS.

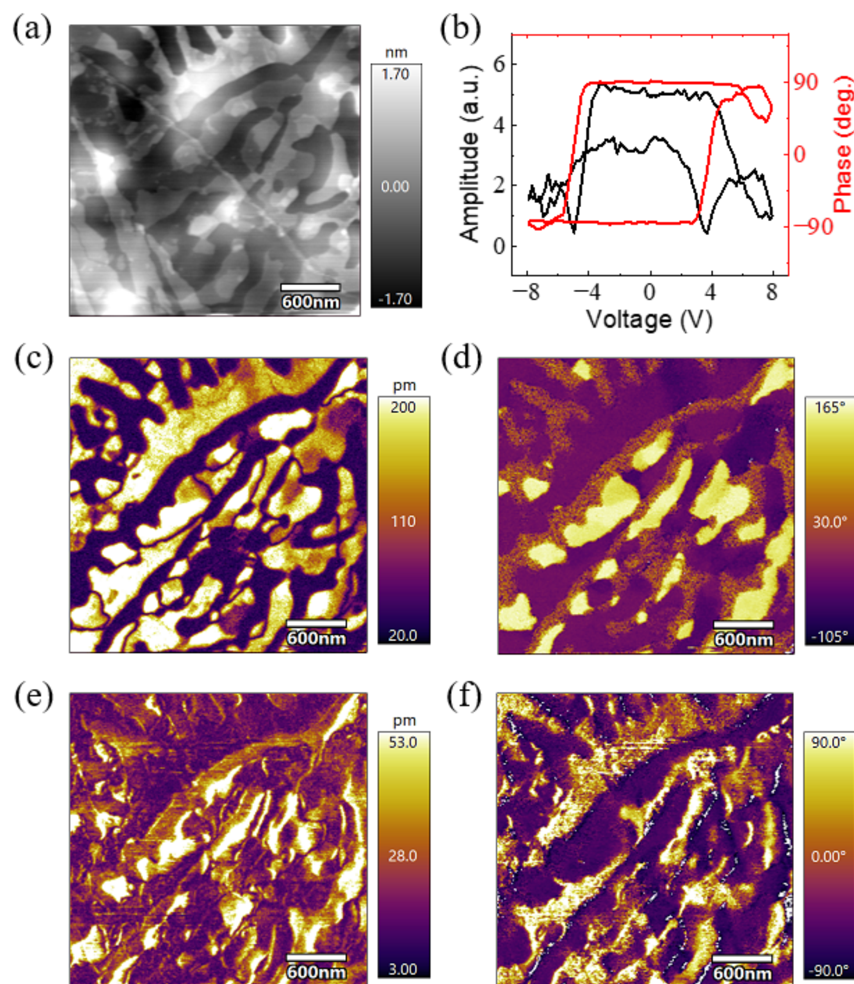

Figure 2. PFM measurements of CIPS flakes. (**a**) The topography of exfoliated CIPS flakes. (**b**) The out-of-plane PFM amplitude (left axis) and phase (right axis) switching hysteresis of 110 nm CIPS flakes. The out-of-plane PFM amplitude (**c**) and phase (**d**) images of CIPS flakes. The in-plane PFM amplitude (**e**) and phase (**f**) images of CIPS flakes.

In order to elucidate the electrode effect on the Schottky-like barrier, the symmetric heterostructure of Au/CIPS/Au was designed, as shown in Figure 4a. The inset of Figure 4a displays the corresponding optical image of the Au/CIPS/Au heterostructure. The typical characteristic I–V curves are shown in Figure 4b, measured at a ramping rate of 0.5 V/s. Generally, the measured current was in the tens of picoamperes, confirming the insulating CIPS. A clear hysteresis loop with a current of ~80 pA was observed under the voltage of ±1.5 V, which was recognized as the volatile resistance switching character. The current switching ratio (I_{on}/I_{off}), defined as the current difference at +0.9 V between the voltage

ramping up and down at the positive voltage branch, was 8.7, which was lightly smaller than that of the Ti/CIPS/Au heterostructure. The hysteresis I–V and the rectifying character appeared with a ramping rate as slow as 2.0 V/s (shown in Figure 4c), which was different compared with that of the Ti/CIPS/Au structure due to symmetric electrode-modulated Schottky-like barriers at the metal/interface.

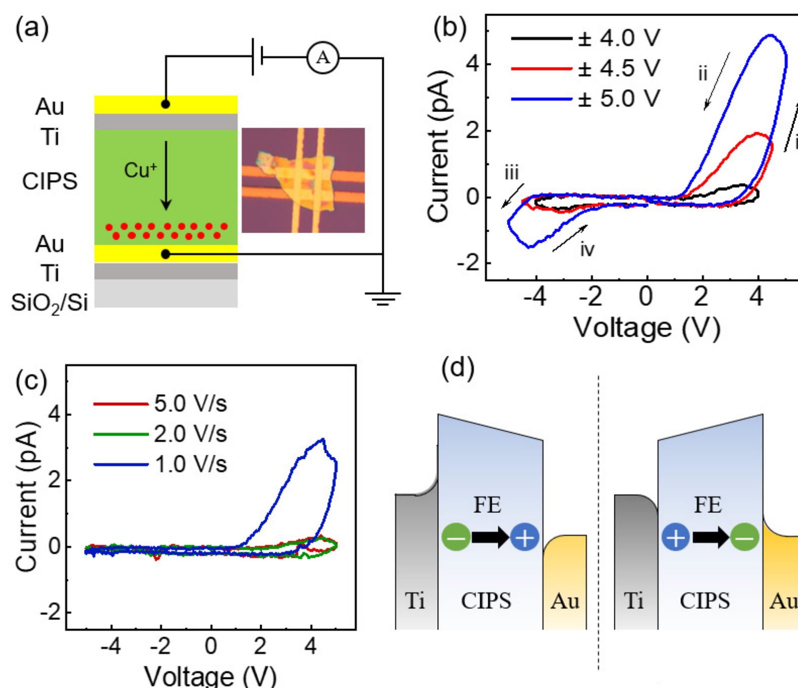

Figure 3. Electrical characterization of Ti/CIPS/Au ferroelectric heterostructure. (**a**) Schematic illustration of Ti/CIPS/Au heterostructure. The inset shows the optical image of fabricated Ti/CIPS/Au. (**b**) The I–V curves measured at various voltages with a ramping rate of 0.2 V/s. The i–iv with arrows indicate the voltage sweeping sequence. (**c**) The I–V curves measured at different ramping rates (1.0 V/s, 2.0 V/s, 5.0 V/s). (**d**) Schematic band alignment of the Ti−CIPS−Au ferroelectric heterostructure.

The nearly symmetric hysteresis I–V loop was observed in the symmetric Au/CIPS/Au heterostructure, which was obviously different from the asymmetric I–V loop in the asymmetric Ti/CIPS/Au. Meanwhile, the rectifying character was clearly displayed both in positive and negative voltage regions, indicating the appearance of symmetric Schottky-like barriers at both Au/CIPS interfaces. The calculated Schottky-like barriers were around 0.895 eV at the two Au/CIPS interfaces, which was slightly smaller compared with the asymmetric Ti/CIPS/Au heterostructure due to the Cu migration. Additionally, the ferroelectric polarization of CIPS could also modulate the interfacial barrier height to some degree (Figure 4d). It should be noted that the thickness of CIPS was around 31 nm for the symmetric Au/CIPS/Au structure. The comparative thin CIPS thickness could have a limited effect on the current amplitude [5]. It seemed that a higher Schottky-like barrier in the Ti/CIPS interface could facilitate the appearance of the hysteresis I–V loop.

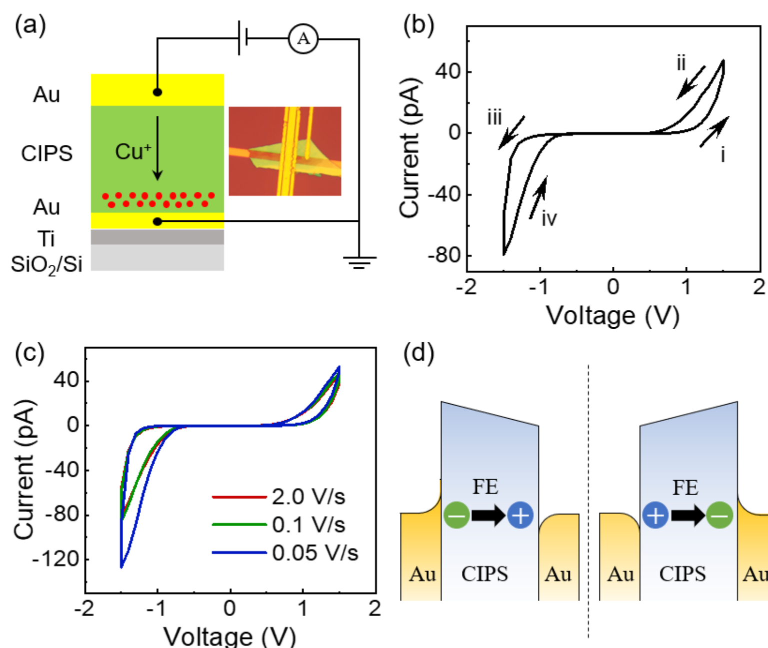

Figure 4. Electrical characterization of Au/CIPS/Au ferroelectric heterostructure. (**a**) Schematic illustration of Au/CIPS/Au ferroelectric structure. The inset shows the optical image of fabricated Au/CIPS/Au structure. (**b**) The I–V curves measured at ±1.5 V with a ramping rate of 0.2 V/s. The i–iv with arrows indicate the voltage sweeping sequence. (**c**) The I–V curves measured at different ramping rates (0.05 V/s, 0.1 V/s, 2.0 V/s). (**d**) Schematic band alignment of the Au−CIPS−Au ferroelectric heterostructure.

4. Conclusions

In summary, the CIPS flakes were exfoliated from the CVT-grown high-quality single crystals, which was testified by X-ray diffraction and Raman spectroscopy. The dominant out-of-plane ferroelectric polarization was verified by piezoresponse force microscopy as well as minor in-plane polarization. The clear hysteresis I–V loops, as well as the rectifying character, were reported in the metal/CIPS/metal heterostructure due to the voltage-induced copper migration, ferroelectric polarization, and carrier (ion) trapping/detrapping at the metal/CIPS interface. In addition, a near symmetric hysteresis I–V loop was displayed in the symmetric Au/CIPS/Au structure, while an asymmetric I–V loop was observed in the Ti/CIPS/Au structure. The higher Schottky-like barrier in the Ti/CIPS interface could facilitate the appearance of the hysteresis I–V loop. The metal electrode could significantly change the Schottky-like barrier, as well as affect the ion migration. This work may facilitate the metal electrode selection for the ferroelectric-based device application.

Author Contributions: Y.D.: Investigation, Visualization, Formal Analysis, Writing—Original Draft; C.A.: Investigation, Visualization, Formal Analysis, Review and Editing; Y.W.: Resources, Investigation, Formal Analysis, Review and Editing; Z.Z.: Investigation, Formal Analysis, Review and Editing; T.L.: Resources, Investigation, Formal Analysis, Review and Editing; T.M.: Resources, Investigation, Formal Analysis, Review and Editing; J.Y.: Investigation, Formal Analysis, Review and Editing; X.C.: Conceptualization, Supervision, Funding Acquisition, Writing—Original Draft; M.T.: Conceptualization, Supervision, Writing—Review and Editing. All authors have read and agreed to the published version of the manuscript.

Funding: This work was supported by the National Natural Science Foundation of China (Grant No. 12104005), the Scientific Research Foundation of the Higher Education Institutions for Distinguished Young Scholars in Anhui Province (Grant No. 2022AH020012), and the Innovation Project for Overseas Researcher in Anhui Province (Grant No. 2022LCX004). This work was also supported by the start-up funding from Anhui University.

Data Availability Statement: The data in this work is available from the corresponding authors upon reasonable request.

Acknowledgments: This work was also supported by the facilities at the Center of Free Electron Laser and High Magnetic Field (FEL&HMF) in Anhui University. We acknowledge the Microscale and Nanoscale Cleanroom at the Center of Quantum Materials in AHU for facilitating the experimental work. We thank the intensive discussions with Xue Liu and Wenshuai Gao in Anhui University and the help from Xiangde Zhu in the High Magnetic Field Laboratory, Chinese Academy of Sciences.

Conflicts of Interest: The authors declare no conflict of interest.

References

1. Si, M.; Liao, P.-Y.; Qiu, G.; Duan, Y.; Ye, P.D. Ferroelectric Field-Effect Transistors Based on MoS_2 and $CuInP_2S_6$ Two-Dimensional van der Waals Heterostructure. *ACS Nano* **2018**, *12*, 6700–6705. [CrossRef] [PubMed]
2. Wang, X.; Yu, P.; Lei, Z.; Zhu, C.; Cao, X.; Liu, F.; You, L.; Zeng, Q.; Deng, Y.; Zhu, C.; et al. Van der Waals negative capacitance transistors. *Nat. Commun.* **2019**, *10*, 3037. [CrossRef]
3. Wu, J.; Chen, H.-Y.; Yang, N.; Cao, J.; Yan, X.; Liu, F.; Sun, Q.; Ling, X.; Guo, J.; Wang, H. High tunnelling electroresistance in a ferroelectric van der Waals heterojunction via giant barrier height modulation. *Nat. Electron.* **2020**, *3*, 466–472. [CrossRef]
4. Wang, C.; Jin, K.-J.; Xu, Z.-T.; Wang, L.; Ge, C.; Lu, H.-B.; Guo, H.-Z.; He, M.; Yang, G.-Z. Switchable diode effect and ferroelectric resistive switching in epitaxial $BiFeO_3$ thin films. *Appl. Phys. Lett.* **2011**, *98*, 192901. [CrossRef]
5. Li, B.; Li, S.; Wang, H.; Chen, L.; Liu, L.; Feng, X.; Li, Y.; Chen, J.; Gong, X.; Ang, K.W. An Electronic Synapse Based on 2D Ferroelectric $CuInP_2S_6$. *Adv. Electron. Mater.* **2020**, *6*, 2000760. [CrossRef]
6. Chen, J.; Zhu, C.; Cao, G.; Liu, H.; Bian, R.; Wang, J.; Li, C.; Chen, J.; Fu, Q.; Liu, Q.; et al. Mimicking Neuroplasticity via Ion Migration in van der Waals Layered Copper Indium Thiophosphate. *Adv. Mater.* **2022**, *34*, e2104676. [CrossRef]
7. Chen, C.; Liu, H.; Lai, Q.; Mao, X.; Fu, J.; Fu, Z.; Zeng, H. Large-Scale Domain Engineering in Two-Dimensional Ferroelectric $CuInP_2S_6$ via Giant Flexoelectric Effect. *Nano Lett.* **2022**, *22*, 3275–3282. [CrossRef] [PubMed]
8. Ming, W.; Huang, B.; Zheng, S.; Bai, Y.; Wang, J.; Wang, J.; Li, J. Flexoelectric engineering of van der Waals ferroelectric $CuInP_2S_6$. *Sci. Adv.* **2022**, *8*, eabq1232. [CrossRef]
9. Ma, R.-R.; Xu, D.-D.; Guan, Z.; Deng, X.; Yue, F.; Huang, R.; Chen, Y.; Zhong, N.; Xiang, P.-H.; Duan, C.-G. High-speed ultraviolet photodetectors based on 2D layered $CuInP_2S_6$ nanoflakes. *Appl. Phys. Lett.* **2020**, *117*, 131102. [CrossRef]
10. Choi, T.; Lee, S.; Choi, Y.J.; Kiryukhin, V.; Cheong, S.W. Switchable Ferroelectric Diode and Photovoltaic Effect in $BiFeO_3$. *Science* **2009**, *324*, 63–66. [CrossRef]
11. Yoshida, C.; Yoshida, A.; Tamura, H. Nanoscale conduction modulation in $Au/Pb(Zr,Ti)O_3/SrRuO_3$ heterostructure. *Appl. Phys. Lett.* **1999**, *75*, 1449–1451. [CrossRef]
12. Won, C.J.; Park, Y.A.; Lee, K.D.; Ryu, H.Y.; Hur, N. Diode and photocurrent effect in ferroelectric $BaTiO_{3-\delta}$. *J. Appl. Phys.* **2011**, *109*, 084108. [CrossRef]
13. Belianinov, A.; He, Q.; Dziaugys, A.; Maksymovych, P.; Eliseev, E.; Borisevich, A.; Morozovska, A.; Banys, J.; Vysochanskii, Y.; Kalinin, S.V. $CuInP_2S_6$ Room Temperature Layered Ferroelectric. *Nano Lett.* **2015**, *15*, 3808–3814. [CrossRef]
14. Liu, F.; You, L.; Seyler, K.L.; Li, X.; Yu, P.; Lin, J.; Wang, X.; Zhou, J.; Wang, H.; He, H.; et al. Room-temperature ferroelectricity in $CuInP_2S_6$ ultrathin flakes. *Nat. Commun.* **2016**, *7*, 12357. [CrossRef] [PubMed]
15. Tsymbal, E.Y.; Kohlstedt, H. Tunneling Across a Ferroelectric. *Science* **2006**, *313*, 181–183. [CrossRef]
16. Tian, B.B.; Liu, Y.; Chen, L.F.; Wang, J.L.; Sun, S.; Shen, H.; Sun, J.L.; Yuan, G.L.; Fusil, S.; Garcia, V.; et al. Space-charge Effect on Electroresistance in Metal-Ferroelectric-Metal capacitors. *Sci. Rep.* **2015**, *5*, 18297. [CrossRef]
17. Maisonneuve, V.; Reau, J.M.; Dong, M.; Cajipe, V.B.; Payen, C.; Ravez, J. Ionic conductivity in ferroic $CuInP_2S_6$ and $CuCrP_2S_6$. *Ferroelectrics* **1997**, *196*, 257–260. [CrossRef]
18. Balke, N.; Neumayer, S.M.; Brehm, J.A.; Susner, M.A.; Rodriguez, B.J.; Jesse, S.; Kalinin, S.V.; Pantelides, S.T.; McGuire, M.A.; Maksymovych, P. Locally Controlled Cu-Ion Transport in Layered Ferroelectric $CuInP_2S_6$. *ACS Appl. Mater. Interfaces* **2018**, *10*, 27188–27194. [CrossRef]
19. Fan, Z.; Fan, H.; Lu, Z.; Li, P.; Huang, Z.; Tian, G.; Yang, L.; Yao, J.; Chen, C.; Chen, D.; et al. Ferroelectric Diodes with Charge Injection and Trapping. *Phys. Rev. Appl.* **2017**, *7*, 014020. [CrossRef]
20. Maisonneuve, V.; Evain, M.; Payen, C.; Cajipe, V.B.; Molinié, P. Room-temperature crystal structure of the layered phase $Cu_IIn_{III}P_2S_6$. *J. Alloys Compd.* **1995**, *218*, 157–164. [CrossRef]
21. Niu, L.; Liu, F.; Zeng, Q.; Zhu, X.; Wang, Y.; Yu, P.; Shi, J.; Lin, J.; Zhou, J.; Fu, Q.; et al. Controlled synthesis and room-temperature pyroelectricity of $CuInP_2S_6$ ultrathin flakes. *Nano Energy* **2019**, *58*, 596–603. [CrossRef]
22. Maisonneuve, V.; Cajipe, V.; Simon, A.; Von Der Muhll, R.; Ravez, J. Ferrielectric ordering in lamellar $CuInP_2S_6$. *Phys. Rev. B* **1997**, *56*, 10860. [CrossRef]
23. Chen, L.; Li, Y.; Li, C.; Wang, H.; Han, Z.; Ma, H.; Yuan, G.; Lin, L.; Yan, Z.; Jiang, X.; et al. Thickness dependence of domain size in 2D ferroelectric $CuInP_2S_6$ nanoflakes. *AIP Adv.* **2019**, *9*, 115211. [CrossRef]

24. Wang, Q.; Xie, T.; Blumenschein, N.A.; Song, Z.; Hanbicki, A.T.; Susner, M.A.; Conner, B.S.; Low, T.; Wang, J.P.; Friedman, A.L.; et al. Gate-tunable giant tunneling electroresistance in van der Waals ferroelectric tunneling junctions. *Mater. Sci. Eng. B* **2022**, *283*, 115829. [CrossRef]
25. Vysochanskii, Y.; Stephanovich, V.A.; Molnar, A.; Cajipe, V.; Bourdon, X. Raman spectroscopy study of the ferrielectric-paraelectric transition in layered $CuInP_2S_6$. *Phys. Rev. B* **1998**, *58*, 9119–9124. [CrossRef]
26. Rao, R.; Selhorst, R.; Conner, B.; Susner, M. Ferrielectric-paraelectric phase transitions in layered $CuInP_2S_6$ and $CuInP_2S_6$–$In_{4/3}P_2S_6$ heterostructures: A Raman spectroscopy and X-ray diffraction study. *Phys. Rev. Mater.* **2022**, *6*, 045001. [CrossRef]
27. Deng, J.; Liu, Y.; Li, M.; Xu, S.; Lun, Y.; Lv, P.; Xia, T.; Gao, P.; Wang, X.; Hong, J. Thickness-Dependent In-Plane Polarization and Structural Phase Transition in van der Waals Ferroelectric $CuInP_2S_6$. *Small* **2020**, *16*, 1904529. [CrossRef]
28. Brehm, J.A.; Neumayer, S.M.; Tao, L.; O'Hara, A.; Chyasnavichus, M.; Susner, M.A.; McGuire, M.A.; Kalinin, S.V.; Jesse, S.; Ganesh, P.; et al. Tunable quadruple-well ferroelectric van der Waals crystals. *Nat. Mater.* **2020**, *19*, 43–48. [CrossRef]
29. Susner, M.A.; Belianinov, A.; Borisevich, A.; He, Q.; Chyasnavichyus, M.; Demir, H.; Sholl, D.S.; Ganesh, P.; Abernathy, D.L.; McGuire, M.A.; et al. High-Tc Layered Ferrielectric Crystals by Coherent Spinodal Decomposition. *ACS Nano* **2015**, *9*, 12365–12373. [CrossRef]
30. Zhou, S.; You, L.; Chaturvedi, A.; Morris, S.A.; Herrin, J.S.; Zhang, N.; Abdelsamie, A.; Hu, Y.Z.; Chen, J.Q.; Zhou, Y.; et al. Anomalous polarization switching and permanent retention in a ferroelectric ionic conductor. *Mater. Horiz.* **2020**, *7*, 263–274. [CrossRef]
31. Jiang, X.; Wang, X.; Wang, X.; Zhang, X.; Niu, R.; Deng, J.; Xu, S.; Lun, Y.; Liu, Y.; Xia, T.; et al. Manipulation of current rectification in van der Waals ferroionic $CuInP_2S_6$. *Nat. Commun.* **2022**, *13*, 574. [CrossRef] [PubMed]
32. Zhang, D.; Luo, Z.-D.; Yao, Y.; Schoenherr, P.; Sha, C.; Pan, Y.; Sharma, P.; Alexe, M.; Seidel, J. Anisotropic Ion Migration and Electronic Conduction in van der Waals Ferroelectric $CuInP_2S_6$. *Nano Lett.* **2021**, *21*, 995–1002. [CrossRef] [PubMed]
33. Zou, X.; Ong, H.G.; You, L.; Chen, W.; Ding, H.; Funakubo, H.; Chen, L.; Wang, J. Charge trapping-detrapping induced resistive switching in $Ba_{0.7}Sr_{0.3}TiO_3$. *AIP Adv.* **2012**, *2*, 032166. [CrossRef]

Disclaimer/Publisher's Note: The statements, opinions and data contained in all publications are solely those of the individual author(s) and contributor(s) and not of MDPI and/or the editor(s). MDPI and/or the editor(s) disclaim responsibility for any injury to people or property resulting from any ideas, methods, instructions or products referred to in the content.